Understanding RNA Chaperone Activity of ProQ Protein

Shilpi Singh, Nisha Kumari, Tanmay Dutta, and Tarak Karmakar*

Department of Chemistry, Indian Institute of Technology, Delhi,

Hauz Khas, New Delhi 110016, India

E-mail: tkarmakar@chemistry.iitd.ac.in

Abstract

RNA-binding proteins (RBPs) are crucial in recognizing and binding small RNAs that modulate gene expression. RBPs often act as RNA chaperones facilitating the sRNA-mRNA duplex formation. One of the most studied sRNA chaperones is Hfq, the post-transcriptional gene regulator in bacteria. Recently a new RNA-chaperone protein, ProQ has been discovered, which binds to a novel sRNA *RaiZ*, derived from the 3'-end of mRNA encoding ribosome-inactivating protein, and promotes its base pairing with the ribosome binding site of hupA mRNA leading to the repression of HU-α protein synthesis. Despite these studies, the RNA binding mechanism in ProQ has not been well explored in detail to date. In this work, we studied the binding of *raiZ* RNA to ProQ using atomistic long-timescale molecular dynamics and on-the-fly probability-based enhanced sampling (OPES) simulations. The *raiZ* RNA binds to ProQ's concave surface mostly decorated with polar and positively charged residues like arginine and lysine exerting electrostatic stabilization to the RNA. *In-silico* mutations of these crucial residues lead to significant loss of the intermolecular interactions resulting in the detachment of the RNA from the protein. The free energy surface obtained from the OPES simulation helps identify stable *raiZ* bound ProQ structures as well as intermediate states. The pertinent atomistic insights into the protein-RNA interactions and deciphering the binding mechanism of the *raiZ* RNA to ProQ enrich our knowledge about ProQ and its RNA chaperone activity.

1. Introduction

RNA-protein interactions play a pivotal role in many physiological processes in all domains of life.[1] The outcome of these interactions includes the transfer of genetic information from DNA to proteins and the regulation of gene expression circuits in the cell.[2,3] Among the many RNAs, a class of regulatory RNAs in bacteria termed small RNAs (sRNAs) finetune the gene expression[4,5] in the cell to help them adapt to changing environments.[6] Small RNAs primarily modulate the gene expression at the post-transcriptional level through base pairing to their cognate targets, and in many instances, require a chaperone protein. One of these extensively characterized matchmaker proteins that promote sRNA-mRNA base pairing is Hfq.[7] However, recent studies using Grad-seq[8], CLIP-seq[9], and RIP-seq10 identified a new RNA-chaperone protein ProQ[11], which was although identified earlier as an osmoregulatory factor obligatory for the expression of proline transporter protein ProP in *Escherichia coli*[12], its RNA-binding capability had never been examined.

The initial indication of the RNA binding activity of ProQ stemmed from the structural similarities of its N-terminal domain (NTD) with the crystal structure of an RNA binding protein (RBP) Fertility inhibitor O (*FinO*). Subsequent ProQ RNA interactome studies have established ProQ as an RBP[13], which acts as a bacterial RNA chaperone[14] and binds largely to a different set of *trans*-acting sRNAs that bind to Hfq.[15] The higher affinity of ProQ for double-stranded RNA indicates that RNA with stem-loop structure(s) is a major determinant for ProQ binding to it. However, not all sRNAs with stem-loop structure(s) have been observed to bind ProQ. This points to additional structural specificities of sRNAs for ProQ binding. Investigations on the ProQ-bound sRNAs revealed that ProQ binds to the 3'-terminus of sRNAs comprising a prerequisite stem-loop followed by a single-stranded poly-Uracil (U) stretch. The 3'-end

stem-loop of sRNA with less than two U residues is unable to bind to ProQ, which instigates an understanding of the mechanism of how ProQ interacts with sRNA and eventually promotes its binding to target mRNA.

ProQ comprises two globular domains connected through an elongated bridging intradomain flexible linker. The N-terminal FinO-like domain possesses RNA binding activity, while the C-terminal domain (CTD) consists of a Tudor domain fold which acts to interpose protein-protein interactions.[16] Although NTD of ProQ has been reported to bind independently to sRNAs, coordinated interactions from NTD, CTD and linker domain of ProQ are necessary for an out-and-out binding to sRNAs as NTD alone is insufficient to bind some typical sRNAs. Knowledge of the mode of interaction of ProQ with sRNA ligands is inadequate as only a handful of studies have been conducted so far to understand the mechanism completely. ProQ has been shown to bind a novel sRNA, *raiZ* derived from the 3'-end of *raiA* mRNA encoding ribosome-inactivating protein, and promotes its base pairing with the ribosome binding site of *hupA* mRNA leading to the repression of HU-α protein synthesis.[17] Of the few other ProQ-sRNA interaction studies, the one that demonstrated that ProQ binds two different sRNA ligands, *rbsZ* and *rybB*, together and facilitates their base pairing interaction[18], happens to follow a distinct mechanistic pathway. The lack of ample experimental studies to establish the ProQ binding mechanism to sRNAs drove us to investigate the mechanism of ligand binding to ProQ systematically.

In this work, we have investigated the binding mechanism of a small RNA *raiZ* to the ProQ N-Terminal (Figure 1a) using extensive atomistic molecular dynamics (MD) and on-the-fly probability-based enhanced sampling (OPES) simulations.[19] The *raiZ* binds to the concave surface of the protein in a semi-folded state. Strong electrostatic interactions between the

positively charged residues such as ARG, HIS, LYS, and the backbone phosphate group of *raiZ* help the guest bind in the ProQ pocket. The RNA binding mechanism and the thermodynamics of the binding process have been studied using OPES simulations using Deep-TDA collective variable (CV)[20] that can constructively capture binding and unbinding events of ProQ-*raiZ*. Furthermore, we performed *in silico* point mutations of important amino acids, ARG80, ARG62, ARG58, and ARG34 (Figure 1b); mutating them to ALA resulted in the unbinding of *raiZ* from the ProQ binding pocket.

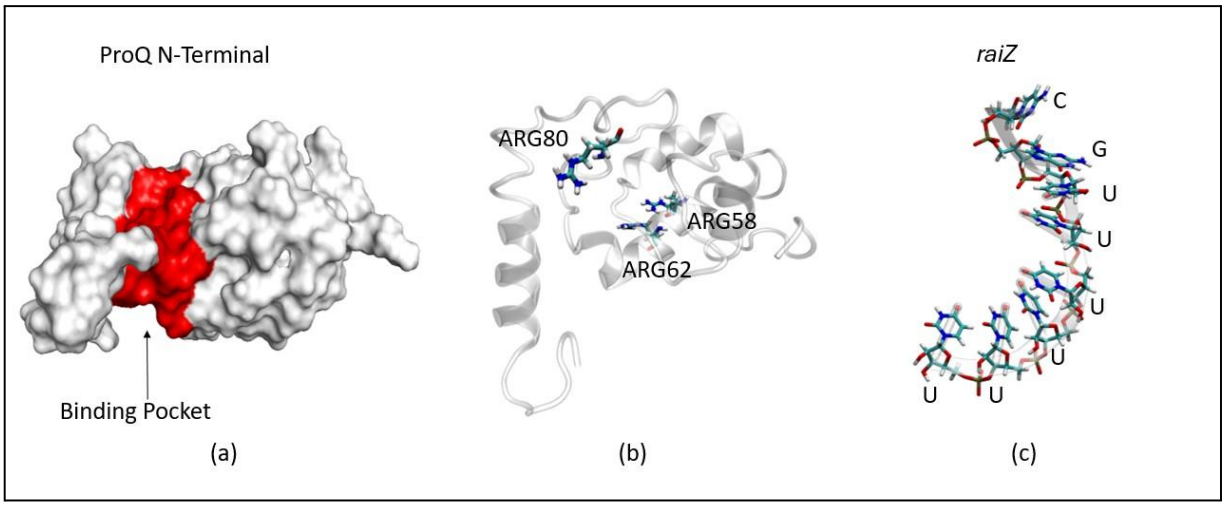

Figure 1: (a) ProQ N-Terminal (surface representation) (PDB ID: 5nb9), the red highlighted region shows binding pocket of ProQ, (b) ProQ N-Terminal (cartoon representation) shows important ARG residues (ARG 58, ARG 62, and ARG 80) for binding *raiZ*, and (c) 3' end of sRNA *raiZ* consist of 8 nucleotides 5'-CGUUUUUU-3'

2. Result & Discussion

2.1. Conformational flexibility of ProQ and *raiZ*

To understand the conformational behavior of ProQ, we carried out an equilibrium MD simulation of a single ProQ-NTD in water. Backbone root mean square deviations (RMSDs) show that ProQ retains its structural integrity throughout the simulation time (Figure S1-a in SI). The high value of RMSD is because of the flexible loops (residues 1-12 and 110-117) present in the ProQ structure. We subsequently conducted an MD simulation of an eight-nucleotide segment of *raiZ* small RNA (5'-CGUUUUUU-3') to elucidate its conformational behavior in water. We selected the 8-nucleotide-long *raiZ* because its 3' end contains more than two uracils, which are crucial for binding, and it is part of the stem-loop. In Figure S1b, the RMSD fluctuations are due to the free extended structure of *raiZ;* no secondary structure of *raiZ* has been observed to form during this simulation.

2.2 *raiZ* binding modes and the stability of ProQ-*raiZ* complex

Once we comprehended the individual behavior of ProQ and *raiZ* in water, our curiosity was heightened to investigate the behavior of the ProQ-*raiZ* complex. Unfortunately, the crystal structure of the *raiZ*-bound ProQ structure is not available. We docked the *raiZ* into ProQ using AutoDock Vina software[21] and obtained a few representative structures of the ProQ-*raiZ* complex, each with varying binding energy values (Table S1 in SI). The structure with the highest binding energy was subjected to a 10 μs-long MD simulation to check the complex's stability and conformational behavior.

From the MD simulation trajectory, we found that the *raiZ* is tightly attached to the concave surface of ProQ, resulting in the formation of a distinctive w-shaped structure of *raiZ* RNA (State-1) (Figure 2a). Our investigation examined the intermolecular interactions that stabilize the *raiZ* RNA on the ProQ surface. The RNA is stabilized on the ProQ surface by electrostatic interactions between the positively charged amino acid residues ARG32-U7, ARG69-U3, ARG109-C1, and ARG80-U8 and the *raiZ's* negatively charged backbone. In addition, the RNA in the ProQ-*raiZ* complex is further stabilized by hydrogen bonds formed between PRO76-U8, SER26-U6, GLN118-U5, TRP68-G2, and TYR78-U3. From the MD simulation trajectory, we observed that the *raiZ* changes its position after about 2.7 microseconds (as shown in Figure 2b).

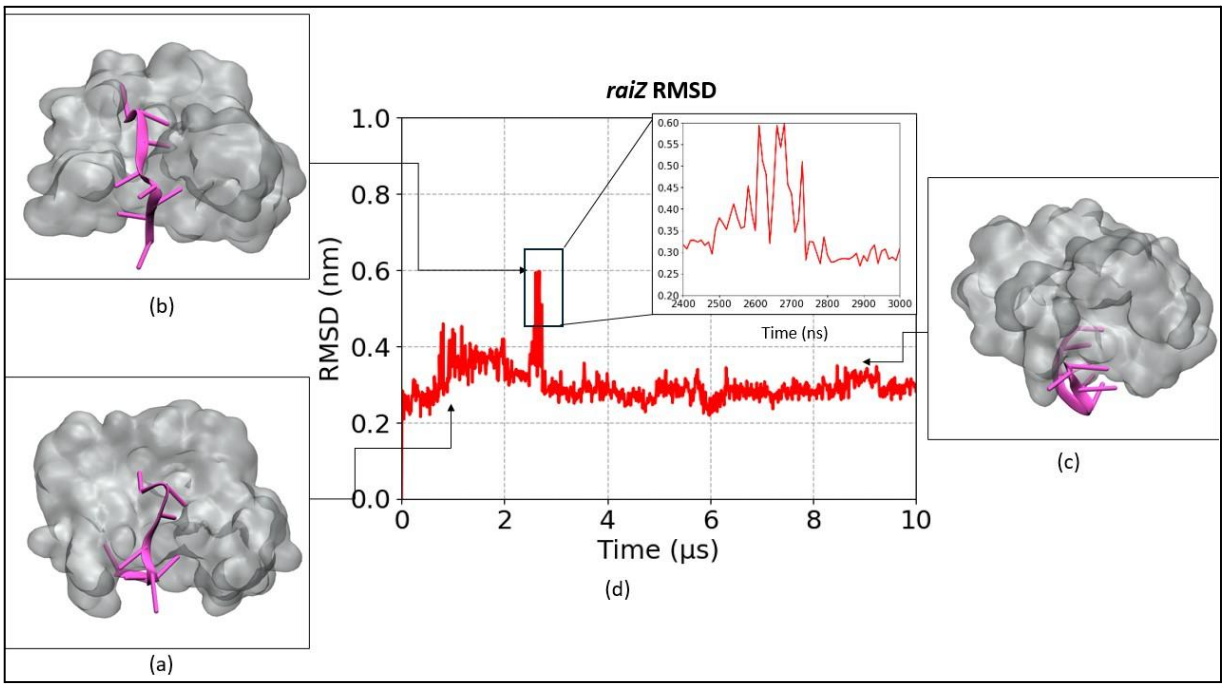

Figure 2: (a) Binding poses of *raiZ* inside ProQ pocket in State-1 (b) intermediate state shows switch from State-1 to State-2 (C) Binding poses of *raiZ* inside ProQ pocket in State-2 (d) RMSD of *raiZ* bound to ProQ

These changes are accompanied by a notable rise in the *raiZ* backbone RMSD. As a result of this change in the position of *raiZ*, the interactions in State-1 (Figure 2a) were disrupted, causing it to transition towards the second conformation state, State-2 (Figure 2c). In State-2, *raiZ* adopted a loop-shaped structure and attached to the lower side of the ProQ protein. Specifically, the 3' end of *raiZ* is bound to the lower back side residues of ProQ. As a result, new hydrogen bonds were formed between ProQ and *raiZ*. Electrostatic interactions occurred between positively charged amino acid residues and the RNA backbone involving PHE39-C1, SER59-U8, GLN111-U7, ARG58-C1, ARG58-G2, ARG109-U3, and ARG62-U6, contribute to the stability of *raiZ* in State-2. The *raiZ* stayed attached to the ProQ in this state throughout the rest of the simulation time. The RMSF analysis (Figure S2 in SI) reveals that in the raiz-ProQ complex, the amino acids residues 30-70, located in the binding site of State-1, have relatively higher RMSF values indicating their possible role in reorganizing *raiZ* in the binding pocket.

2.3. *In silico* mutations – the role of pocket residues

From the unbiased simulation, we have found that in State-1, two ARG residues, ARG80 and ARG32 present inside the binding pocket stabilize the *raiZ*. Similarly, in State-2, ARG58 and ARG62 occupy the binding pocket and hold *raiZ* (Figure 3). To further understand the role of these amino acids in the *raiZ* binding, we have carried out *in-silico* mutational studies. We conducted two different sets of mutations, (i) R80A and (ii) R32A in State-1 and (iii) R58A-R62A double mutant, (vi) R58A, (v) R62A in State-2 and calculated the distance between Cα of amino acid and RNA backbone atom of mutants and compared them with that of the wild type (WT) protein.

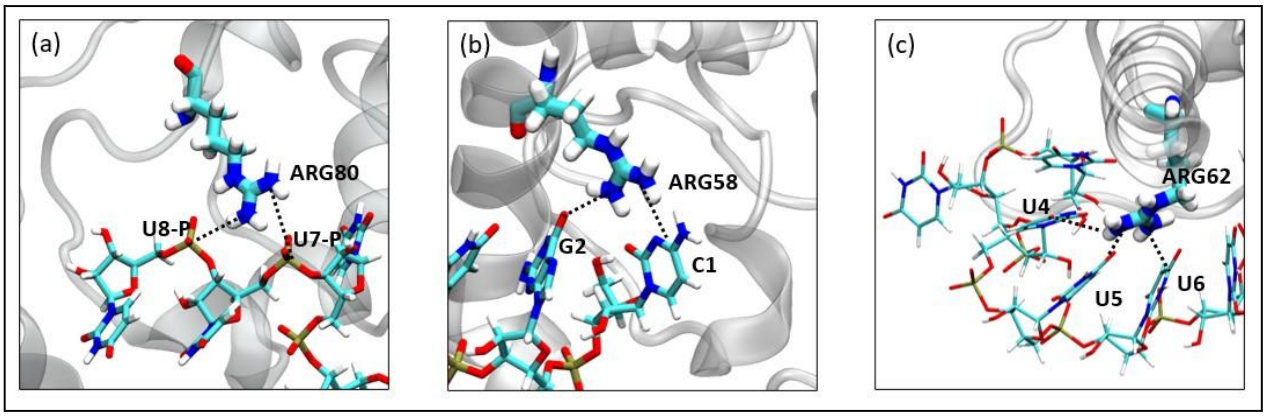

Figure 3: (a) Electrostatic interactions between the side chain of ARG80 and phosphate of U7 and U8 of *raiZ*, (b) cation-π interactions between the side chain of ARG58 with C1 and G2 of *raiZ*, and (c) cation-π interactions between the side chain of ARG62 and U4, U5, and U6 of *raiZ*.

The core residue, ARG80 has been reported to have a significant role in RNA binding.[22] Owing to its positive charge, ARG80 interacts strongly with the *raiZ* RNA backbone phosphate group and helps bind the RNA inside the ProQ concave surface. Pandey *et al.*[22] carried out mutational studies on this residue and found out that the mutation of this highly conserved basic residue ARG80 to ALA strongly reduces interactions with cspE and sibB hybrid RNAs in B3H assay (protein-RNA interaction assay) leading to binding affinity of RNA with ProQ. As expected, the MD simulation of the R80A mutant with *raiZ* showed increased RMSD of the RNA compared to that in the WT (Section 2, Figure S3 in SI). In particular, the distance measuring the contact between ALA80 Cα and U8 showed large deviations in the mutant compared to that in the WT (Figure 4c), indicating that RNA is loosely bound in the mutant (Figure 4a). Similarly, we have observed another core residue ARG32 bound to *raiZ* has a significant role (Section 2, Figure S5

in SI) ARG80 and ARG32 interact with RNA residues in a zipper-like fashion and hold the RNA inside the cavity (Figure S4 in SI).

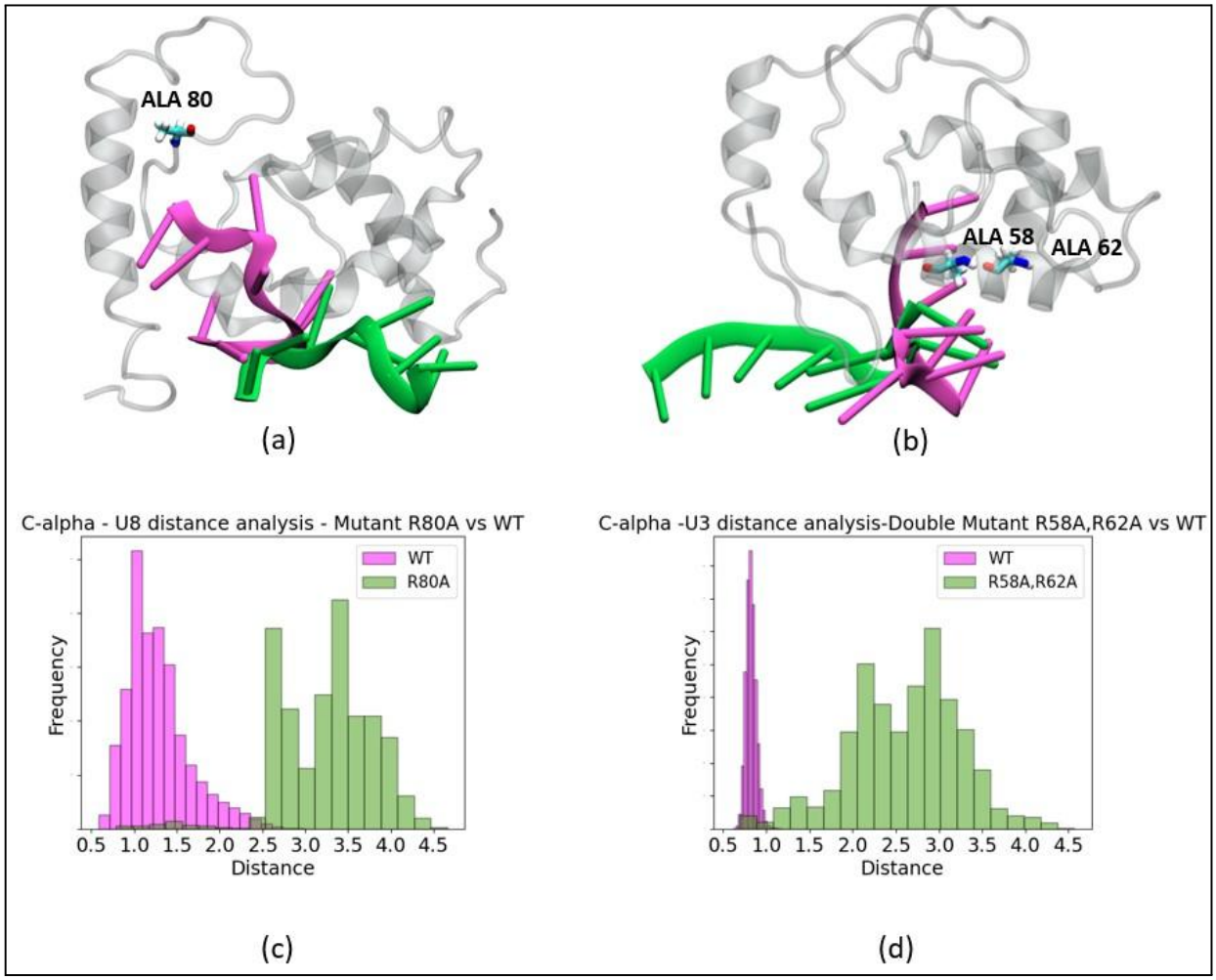

Figure 4: (a) *raiZ* binding position in State-1 for WT (magenta) *vs*. R80A mutant (green), (b) *raiZ* binding position in State-2 for WT (magenta) *vs.* R58A-R62A double mutant (green) (c) Histogram showing Cα-U8 contact distance distribution throughout the trajectory in WT (magenta) and R80A mutant (green) (d) Histogram showing Cα-U3 contact distance distribution throughout the trajectory in WT (magenta) and R58-62A mutant (green)

Upon visually inspecting the trajectory, we identified that in State-2, two arginine residues, ARG58 and ARG62, located on the bottom side of ProQ and in proximity, contribute to the holding of *raiZ* within the pocket. We performed MD simulations of three mutations: R58A, R62A, and a double mutant R58A-R62A complexed with *raiZ*. Our findings suggest these mutations significantly influence RNA binding with ProQ. In the case of a single mutation, either R58A or R62A, there is no considerable change in the position of the *raiZ*; it stays inside the binding pocket. This is evident due to the presence of the adjacent non-mutated ARG58 or ARG62 is enough to retain the RNA within the pocket. However, in the double mutant R58A-R62A, the *raiZ* comes out of the binding pocket within a few ns (Figure 4b). To confirm this, we computed the distance between the Cα of ALA58 and U3, as seen in Figure 4d. The distance between ARG58 and U3 in the WT histogram ranges from 0.2 to 1.0 Å. Notably, in the R58A-R62A double mutation, the same distance increases significantly, ranging from 2.0 to 4.5 Å, indicating the unbinding of *raiZ* from ProQ.

2.4 Spontaneous Binding of *raiZ* with ProQ

Thus far, we have utilized a pre-docked ProQ-*raiZ* complex for our simulation studies. However, to get a comprehensive understanding of the binding process of our system, we must analyze our system from alternative perspectives as well. In this case, we conducted a spontaneous binding simulation (SBS) without any predetermined coordinates or path to explore other binding pockets of ProQ. We conducted multiple independent MD simulations, starting with different initial configurations of the ProQ-*raiZ* complex. For these simulations, we manually positioned the target RNA at varying distances (30-45 Å) and orientations relative to the ProQ. Multiple

SBS results were presented in this study. The first outcome, depicted in (Figure S6 (a-1) in SI), shows that the *raiZ* is positioned approximately 45 Å away from the protein. Initially, the *raiZ* was freely floating around, however, after a few nanoseconds, it began to approach the protein. This movement was primarily driven by long-range electrostatic interactions between positively charged amino acids and the negatively charged backbone of the *raiZ*. Eventually, the *raiZ* got attached to the lower end of the ProQ, as shown in (Figure S6 (a-2) in SI).

In the second simulation, *raiZ* was positioned approximately 33 Å away from the ProQ on the upper side (Figure S6 (b-1) in SI). Initially, the *raiZ* attached to the front side of the ProQ is driven solely by electrostatic interactions, exploring other conformations over the protein surface. After some time, it started moving closer to the backside of the ProQ and ultimately got attached there in a relatively stable conformation compared to other conformations shown in (Figure S6(b-1) in SI).

2.5 ProQ-*raiZ* binding thermodynamics and mechanism

The equilibrium MD simulations including SBS provided pertinent atomistic insights into the binding interactions between the ProQ and *raiZ*. However, when delineating the RNA binding mechanism, equilibrium MD simulations find limitations due to the limited sampling time. We anticipate that *raiZ* binding to ProQ involves a much larger timescale which standard brute-force MD simulations cannot sample. To circumvent this timescale limitation, we carried out On-the-fly Probability Enhanced Sampling (OPES) simulations[19]. We utilized the recently developed Deep-TDA method[23] to design a collective variable (CV) based on 26 contact pairs between the ProQ and *raiZ* (Figure S7 in SI). In particular, we included many short and

long-range contacts, including H-bonds, as descriptors for the DeepTDA method (see Methods section). Along with this Deep-TDA CV, we defined the backbone RMSD of *raiZ* as the second CV(s_2). The use of Deep TDA along with a physical CV has been found effective in studying biomolecular recognition.[24]

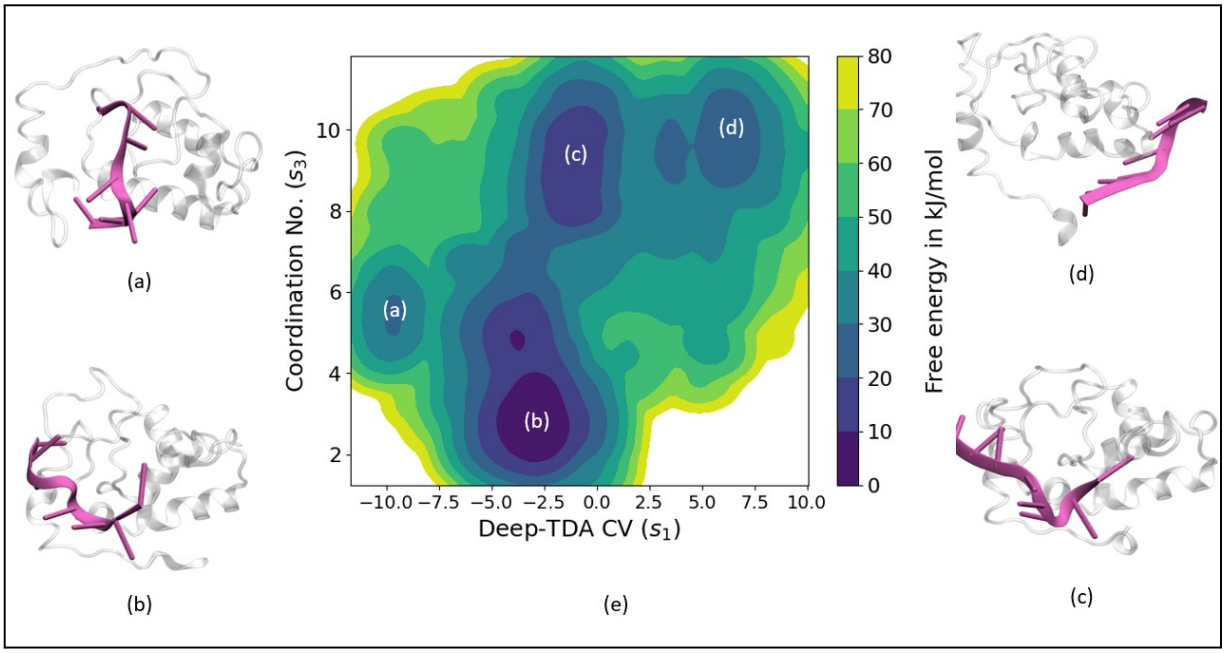

Figure 5: Free Energy Surface (FES) diagram with different metastable states - basin (a): initial bound state (State-1), basin (b): the deepest basin corresponding to the the raiZ bound state in the same binding pocket but with a different orientation, basin (c): intermediate state similar to the basin (b) but having less contact with ProQ and having high CN represent more soluble with water also loosely bind to ProQ, basin (d): almost unbound state having very fewer contacts with ProQ and highly soluble with water as the higher value of CN, (e) the free energy surface (FES) as a function of s_1 and s_3 CVs.

With these two CVs, s_1 and s_2, we carried out an OPES simulation to study the binding and unbinding mechanism of the ProQ-*raiZ* complex and explore possible metastable states, which are often inaccessible from equilibrium MD simulations due to the high energy barrier between the two metastable states. In the 2.5 μs OPES simulation, we observed a few back-and-forth transitions between the *raiZ*-bound state (-10) and unbounded state (10). (Figure S8 in SI) Using a reweighting method[19], we calculated the free energy surface (FES) as a function of the Deep-TDA CV(s_1) and another CV(s_3) based on the coordination number of water (*j*=oxygen) surrounding an atom (1) at the center of *raiZ,* defined as,

$$s_3 = \sum_{1j} \frac{1 - (\frac{r_{1j}}{r_0})^n}{1 - (\frac{r_{1j}}{r_0})^m}$$

Here, r_{1j} denotes the contact distance between the atom (*1)* of raiZ and oxygen atoms *(j)* of water, while r^0 is a reference distance, set to 0.4 nm, that defines the distance range over which a contact is considered significant; *n* and *m* are parameters of the switching function. The rationale for considering the third CV(s_3) is that it could differentiate the basins well but cannot efficiently sample them due to possible hysteresis.

In Figure 5, the basin (a) represents the conformation having the maximum number of contacts between ProQ and *raiZ* according to our Deep-TDA CV and CN around 5 with water molecules around the binding pocket, this conformation is the same as State-1 which we initially conjectured as the binding pose of *raiZ* complexed with ProQ. Due to the high flexibility of the *raiZ* backbone and also the flexible loop region around the binding pocket of ProQ protein, *raiZ* explores many other metastable states having free energy values ranging from 0-80 kJ/mol as shown in (Figure 5e). By thoroughly analyzing all these metastable states (basins) on the FES we

found the possible pathway of *raiZ* binding to ProQ and subsequent folding. During unbinding, with the bias deposited in basin (a), the *raiZ* moves to a more stable basin (b) in which it remains attached to the same concave surface but in a different orientation compared to basin (a). Further deposition of bias in the basin (b) leads to detachment of the RNA from the protein and following basin (c) and (d) *raiZ* finally detaches completely from the ProQ surface and attains the unbound state. Similarly, during re-binding, it starts from basin (d) where positive amino acids attract the negatively charged *raiZ* and loosely bind the RNA. This is followed by the binding of *raiZ* to the lower side of ProQ, basins (c) and (d). Subsequently, *raiZ* starts to approach the binding pocket basin (b) in which positive amino acids ARG80, ARG58, ARG62, ARG109, and ARG100 mediate the binding process. Eventually, *raiZ* fits inside the binding pocket of ProQ and attains state (b) which is more stable than State-1 of the basin (a) obtained from docking. To characterize these basins further, we have carried out short ~200-400 ns simulations starting from a configuration in each basin. From these trajectories, we calculated the two CV values and projected them on the FES. The trajectories sample the corresponding basin indicating that the basins are intermediate states connecting the *raiZ* bound and the unbound states. (Figure S10) To evaluate the convergence of the simulation, we conducted the subsequent tests: we examined the free energy difference (ΔG) as a function of simulation time, as illustrated in (Figure S9 in SI). The plot indicates that the ΔG remains relatively constant after around 1 μs, implying that the free energy has almost converged.

Additionally, to elucidate the chaperone activity of ProQ, we computed the radius of gyration (R_g) profiles of *raiZ* from the unbiased simulations initiated from each of the four basins (a), (b), (c), and (d) of the FES (Figure 5) and compared them with the R_g profile obtained from the simulation of a free *raiZ* in water (Figure S11). As evident from Figure S11, in water, *raiZ*

prefers to stay in the extended conformation stabilized by water solvation, while when bound to ProQ, it gets partially folded indicated by the reduced R_g values. In the most stable basin (b), raiZ has the most compact structure compared to the other basins. This analysis indicates the likely role of ProQ in RNA chaperon activity.

Conclusion

In summary, we have investigated the specific action of ProQ in small RNA *raiZ* binding and subsequent folding. Utilizing long microsecond timescale molecular dynamics (MD) simulations, we found the conformational preferences of *raiZ* RNA on the ProQ's concave-shaped binding pocket and identified positively charged amino acids such as ARG, LYS, and HIS playing a crucial role in holding the RNA inside the binding site and aid in its folding. We identified two possible binding sites - State-1 and State-2. *In-silico* mutational studies revealed the role of ARG80, ARG58, and ARG62 residues in binding *raiZ* in these binding sites. In addition, we utilized OPES simulations to explore the mechanism of *raiZ* binding to ProQ and calculate the free energy landscape. Initially, the *raiZ* interacts with ProQ's surface through its positively charged residues; as conformational fluctuations continue, the *raiZ* gradually approaches the binding site where ProQ folds *raiZ* RNA. Moreover from the Radius of gyration calculation, low values of Rg in the bound state, basin (b) supports RNA Chaperone activity of ProQ. These findings substantially improve our knowledge of ProQ's role as an RNA chaperone and its interaction with small RNAs like *raiZ*. The knowledge gathered from this research serves as a valuable foundation for future investigations conducted in *in-vitro* and *in-vivo* studies. This positions the ProQ-*raiZ* complex as a promising target for the development of new antibiotics.

Methodology

Dataset

We extracted the NMR structure of the N-terminal domain of the Escherichia Coli ProQ RNA binding protein from the RCSB[25] protein data bank (PDB ID: 5NB9; Grecia M. Gonzalez et. al.).[26] Out of 17 models present in the ProQ PDB file, the first model structure was used for this investigation, since it was close to the average structure and also had the lowest energy value among 17 models. For generating sRNA (*raiZ*) 3D structure file, the sequence was downloaded from the web database EcoCyc[27,28] (*raiZ* accession ID: GO-17078). Further, the RNAfold[29] and RNA composer tool[30,31] were used for developing the coordinates in PDB format.

Molecular Docking studies

Molecular docking of the N-terminal domain of the Escherichia Coli ProQ protein, along with sRNA *raiZ* was performed using the AutoDock Vina software[21]. For docking purposes, only 8 nucleoside long sequences of the putative binding site (5'-CGUUUUUU-3'), which is present on the 3' end of the *raiZ*, have been used. The binding affinity was computed for this ProQ-raiZ complex. For the grid box, the XYZ coordinates were set at -1.242, -7.319, and 4.461, respectively, with a grid spacing of 1 Å. The dimensions of the box were set at 80×80×80 with an exhaustiveness value equal to 8 and an energy range of 4. From docking results, we got 9 different binding conformations having different binding affinities, out of which the first conformation was selected having the highest binding affinity equal to -7.5 kcal/mol. This ProQ-raiZ complex has been used for further molecular dynamics studies.

Molecular dynamics simulations:

The structure obtained from the molecular docking result was utilized for molecular dynamics simulation. We carried out three set of simulations - (i) ProQ in water, (ii) putative binding site (5'-CGUUUUUU-3') of *raiZ* in water, and (iii) ProQ-*raiZ* docked complex in water using GROMACS v 2021.4.[32] The AMBER99SB-ILDN force field[33] was used for ProQ. While, for *raiZ*, the OL3[34] nucleic acid force field was used for generating the interaction potentials both in water as well as in complex. In all the systems, the simulation box was solvated using the SPCE water model[35], and ions were added to neutralize the system.[36] Further, the steepest descent algorithm was used to remove the unwanted contacts and bring the system to a minimum energy. Lastly, all three systems were equilibrated, using v-rescale[37] thermostat and Parrinello-Rahman barostat[38] to a target temperature of 300 K and 1 bar pressure, respectively. The production MD was performed using the leap-frog algorithm and equations of motions were integrated after every 2 fs.

Enhanced Sampling Method

We employed the recently developed enhanced sampling method, the On-the-fly Probability Enhanced Sampling (OPES)[19,39] to sample binding and unbinding events and explore a range of possible conformations of the system. The Deep-TDA CV (s_1) along with the raiZ RMSD CV (s_2), were used in the OPES simulations to explore the range of possible conformations of the system. To train the Deep-TDA CV, we took 26 contact pair distances between the Cα atoms of amino acids of the ProQ protein and the backbone atoms of *raiZ* RNA. These contacts were chosen from the equilibrium simulation trajectories. The training was done for two distinct

bound states and one unbound state. Afterward, utilizing these descriptors, the Deep-TDA CV was constructed. The Pytorch40[40] library was utilized for training the model, and subsequently, the trained model from Pytorch was imported into PLUMED utilizing the interface built by Bonati *et al*.[41]. The GROMACS-2021.4[32] patched with PLUMED2.9[42] was utilized to conduct the enhanced sampling (ES) simulations.

Acknowledgments

The authors acknowledge IIT Delhi for the research funding and all necessary facilities. SS and NK thank IITD for their Ph.D. fellowships. T.K. thanks the IITD for the seed grant. The authors extend their appreciation to the IITD HPC for the supercomputing facility (DST-FIST).

Supporting Information

The supporting information contains - Binding affinity of different binding modes obtained from docking of ProQ and *raiZ* using AutoDock, RMSD and RMSF plots, spontaneous binding simulation results, CV profile, FES with projected CV values from unbiased simulations run at each basin of the FES, Rg plot showing ProQ's chaperon activity.

Data Availability Statement

The input files required to run the simulations and results data can be found in the GitHub repository ___

References

(1) Re, A.; Joshi, T.; Kulberkyte, E.; Morris, Q.; Workman, C. T. RNA–Protein Interactions: An Overview. In *RNA Sequence, Structure, and Function: Computational and Bioinformatic Methods*; Gorodkin, J., Ruzzo, W. L., Eds.; Humana Press: Totowa, NJ, 2014; pp 491–521. https://doi.org/10.1007/978-1-62703-709-9_23.

(2) Gerstberger, S.; Hafner, M.; Tuschl, T. A Census of Human RNA-Binding Proteins. *Nat. Rev. Genet.* **2014**, *15* (12), 829–845. https://doi.org/10.1038/nrg3813.

(3) Dutta, T.; Srivastava, S. Small RNA-Mediated Regulation in Bacteria: A Growing Palette of Diverse Mechanisms. *Gene* **2018**, *656*, 60–72. https://doi.org/10.1016/j.gene.2018.02.068.

(4) Portnoy, V.; Huang, V.; Place, R. F.; Li, L.-C. Small RNA and Transcriptional Upregulation. *WIREs RNA* **2011**, *2* (5), 748–760. https://doi.org/10.1002/wrna.90.

(5) Fröhlich, K. S.; Vogel, J. Activation of Gene Expression by Small RNA. *Curr. Opin. Microbiol.* **2009**, *12* (6), 674–682. https://doi.org/10.1016/j.mib.2009.09.009.

(6) Storz, G.; Vogel, J.; Wassarman, K. M. Regulation by Small RNAs in Bacteria: Expanding Frontiers. *Mol. Cell* **2011**, *43* (6), 880–891. https://doi.org/10.1016/j.molcel.2011.08.022.

(7) Global Analysis of Small RNA and mRNA Targets of Hfq.

(8) Hör, J.; Di Giorgio, S.; Gerovac, M.; Venturini, E.; Förstner, K. U.; Vogel, J. Grad-Seq Shines Light on Unrecognized RNA and Protein Complexes in the Model Bacterium Escherichia Coli. *Nucleic Acids Res.* **2020**, *48* (16), 9301–9319. https://doi.org/10.1093/nar/gkaa676.

(9) Stoute, J.; Liu, K. F. CLIP-Seq to Identify Targets and Interactions of RNA Binding Proteins and RNA Modifying Enzymes. *Methods Enzymol.* **2021**, *658*, 419–434. https://doi.org/10.1016/bs.mie.2021.08.001.

(10) Melamed, S.; Faigenbaum-Romm, R.; Peer, A.; Reiss, N.; Shechter, O.; Bar, A.; Altuvia, Y.; Argaman, L.; Margalit, H. Mapping the Small RNA Interactome in Bacteria Using

RIL-Seq. *Nat. Protoc.* **2018**, *13* (1), 1–33. https://doi.org/10.1038/nprot.2017.115.

(11) Identification of Novel Small RNAs Using Comparative Genomics and Microarrays.

(12) *Structural and Functional Analysis of ProQ: An Osmoregulatory Protein of Escherichia coli | Biochemistry*. https://pubs.acs.org/doi/full/10.1021/bi6023786 (accessed 2024-04-30).

(13) *Grad-seq guides the discovery of ProQ as a major small RNA-binding protein | PNAS*. https://www.pnas.org/doi/abs/10.1073/pnas.1609981113 (accessed 2024-04-30).

(14) Woodson, S. A.; Panja, S.; Santiago-Frangos, A. Proteins That Chaperone RNA Regulation. *Microbiol. Spectr.* *6* (4), 10.1128/microbiolspec.rwr-0026–2018. https://doi.org/10.1128/microbiolspec.rwr-0026-2018.

(15) Holmqvist, E.; Berggren, S.; Rizvanovic, A. RNA-Binding Activity and Regulatory Functions of the Emerging sRNA-Binding Protein ProQ. *Biochim. Biophys. Acta BBA - Gene Regul. Mech.* **2020**, *1863* (9), 194596. https://doi.org/10.1016/j.bbagrm.2020.194596.

(16) Stein, E. M.; Kwiatkowska, J.; Basczok, M. M.; Gravel, C. M.; Berry, K. E.; Olejniczak, M. Determinants of RNA Recognition by the FinO Domain of the Escherichia Coli ProQ Protein. *Nucleic Acids Res.* **2020**, *48* (13), 7502–7519. https://doi.org/10.1093/nar/gkaa497.

(17) *Molecular mechanism of mRNA repression in trans by a ProQ‐dependent small RNA | The EMBO Journal*. https://www.embopress.org/doi/full/10.15252/embj.201696127 (accessed a2023-12-12).

(18) Melamed, S.; Adams, P. P.; Zhang, A.; Zhang, H.; Storz, G. RNA-RNA Interactomes of ProQ and Hfq Reveal Overlapping and Competing Roles. *Mol. Cell* **2020**, *77* (2), 411-425.e7. https://doi.org/10.1016/j.molcel.2019.10.022.

(19) Invernizzi, M.; Parrinello, M. Rethinking Metadynamics: From Bias Potentials to Probability Distributions. *J. Phys. Chem. Lett.* **2020**, *11* (7), 2731–2736. https://doi.org/10.1021/acs.jpclett.0c00497.

(20) Kumari, N.; Dhull, S.; Karmakar, T. Enhanced Sampling Simulations of RNA-Peptide Binding Using Deep Learning Collective Variables. bioRxiv August 2, 2024, p

2024.08.01.606277. https://doi.org/10.1101/2024.08.01.606277.

(21) Eberhardt, J.; Santos-Martins, D.; Tillack, A. F.; Forli, S. AutoDock Vina 1.2.0: New Docking Methods, Expanded Force Field, and Python Bindings. *J. Chem. Inf. Model.* **2021**, *61* (8), 3891–3898. https://doi.org/10.1021/acs.jcim.1c00203.

(22) Pandey, S.; Gravel, C. M.; Stockert, O. M.; Wang, C. D.; Hegner, C. L.; LeBlanc, H.; Berry, K. E. Genetic Identification of the Functional Surface for RNA Binding by Escherichia Coli ProQ. *Nucleic Acids Res.* **2020**, *48* (8), 4507–4520. https://doi.org/10.1093/nar/gkaa144.

(23) Trizio, E.; Parrinello, M. From Enhanced Sampling to Reaction Profiles. *J. Phys. Chem. Lett.* **2021**, *12* (35), 8621–8626. https://doi.org/10.1021/acs.jpclett.1c02317.

(24) Kumari, N.; Sonam; Karmakar, T. Enhanced Sampling Simulations of RNA–Peptide Binding Using Deep Learning Collective Variables. *J. Chem. Inf. Model.* **2025**. https://doi.org/10.1021/acs.jcim.4c01438.

(25) Berman, H. M.; Westbrook, J.; Feng, Z.; Gilliland, G.; Bhat, T. N.; Weissig, H.; Shindyalov, I. N.; Bourne, P. E. The Protein Data Bank. *Nucleic Acids Res.* **2000**, *28* (1), 235–242. https://doi.org/10.1093/nar/28.1.235.

(26) Gonzalez, G. M.; Hardwick, S. W.; Maslen, S. L.; Skehel, J. M.; Holmqvist, E.; Vogel, J.; Bateman, A.; Luisi, B. F.; Broadhurst, R. W. Structure of the Escherichia Coli ProQ RNA-Binding Protein. *RNA* **2017**, *23* (5), 696–711. https://doi.org/10.1261/rna.060343.116.

(27) Karp, P. D.; Paley, S.; Caspi, R.; Kothari, A.; Krummenacker, M.; Midford, P. E.; Moore, L. R.; Subhraveti, P.; Gama-Castro, S.; Tierrafria, V. H.; Lara, P.; Muñiz-Rascado, L.; Bonavides-Martinez, C.; Santos-Zavaleta, A.; Mackie, A.; Sun, G.; Ahn-Horst, T. A.; Choi, H.; Covert, M. W.; Collado-Vides, J.; Paulsen, I. The EcoCyc Database (2023). *EcoSal Plus* **2023**, *11* (1), eesp-0002-2023. https://doi.org/10.1128/ecosalplus.esp-0002-2023.

(28) Moore, L. R.; Caspi, R.; Boyd, D.; Berkmen, M.; Mackie, A.; Paley, S.; Karp, P. D. Revisiting the Y-Ome of Escherichia Coli. *Nucleic Acids Res.* **2024**, *52* (20), 12201–12207. https://doi.org/10.1093/nar/gkae857.

(29) Lorenz, R.; Bernhart, S. H.; Höner zu Siederdissen, C.; Tafer, H.; Flamm, C.; Stadler, P. F.;

Hofacker, I. L. ViennaRNA Package 2.0. *Algorithms Mol. Biol.* **2011**, *6* (1), 26. https://doi.org/10.1186/1748-7188-6-26.

(30) Popenda, M.; Szachniuk, M.; Antczak, M.; Purzycka, K. J.; Lukasiak, P.; Bartol, N.; Blazewicz, J.; Adamiak, R. W. Automated 3D Structure Composition for Large RNAs. *Nucleic Acids Res.* **2012**, *40* (14), e112. https://doi.org/10.1093/nar/gks339.

(31) Sarzynska, J.; Popenda, M.; Antczak, M.; Szachniuk, M. RNA Tertiary Structure Prediction Using RNAComposer in CASP15. *Proteins Struct. Funct. Bioinforma.* **2023**, *91* (12), 1790–1799. https://doi.org/10.1002/prot.26578.

(32) Abraham, M. J.; Murtola, T.; Schulz, R.; Páll, S.; Smith, J. C.; Hess, B.; Lindahl, E. GROMACS: High Performance Molecular Simulations through Multi-Level Parallelism from Laptops to Supercomputers. *SoftwareX* **2015**, *1–2*, 19–25. https://doi.org/10.1016/j.softx.2015.06.001.

(33) Hornak, V.; Abel, R.; Okur, A.; Strockbine, B.; Roitberg, A.; Simmerling, C. Comparison of Multiple Amber Force Fields and Development of Improved Protein Backbone Parameters. *Proteins Struct. Funct. Bioinforma.* **2006**, *65* (3), 712–725. https://doi.org/10.1002/prot.21123.

(34) Zgarbová, M.; Otyepka, M.; Šponer, J.; Mládek, A.; Banáš, P.; Cheatham, T. E. I.; Jurečka, P. Refinement of the Cornell et al. Nucleic Acids Force Field Based on Reference Quantum Chemical Calculations of Glycosidic Torsion Profiles. *J. Chem. Theory Comput.* **2011**, *7* (9), 2886–2902. https://doi.org/10.1021/ct200162x.

(35) *The missing term in effective pair potentials | The Journal of Physical Chemistry*. https://pubs.acs.org/doi/10.1021/j100308a038 (accessed 2025-01-11).

(36) Joung, I. S.; Cheatham, T. E. I. Determination of Alkali and Halide Monovalent Ion Parameters for Use in Explicitly Solvated Biomolecular Simulations. *J. Phys. Chem. B* **2008**, *112* (30), 9020–9041. https://doi.org/10.1021/jp8001614.

(37) Bussi, G.; Donadio, D.; Parrinello, M. Canonical Sampling through Velocity Rescaling. *J. Chem. Phys.* **2007**, *126* (1), 014101. https://doi.org/10.1063/1.2408420.

(38) Parrinello, M.; Rahman, A. Polymorphic Transitions in Single Crystals: A New Molecular Dynamics Method. *J. Appl. Phys.* **1981**, *52* (12), 7182–7190. https://doi.org/10.1063/1.328693.

(39) Invernizzi, M.; Piaggi, P. M.; Parrinello, M. Unified Approach to Enhanced Sampling. *Phys. Rev. X* **2020**, *10* (4), 041034. https://doi.org/10.1103/PhysRevX.10.041034.

(40) Paszke, A.; Gross, S.; Chintala, S.; Chanan, G.; Yang, E.; DeVito, Z.; Lin, Z.; Desmaison, A.; Antiga, L.; Lerer, A. Automatic Differentiation in PyTorch. **2017**.

(41) Bonati, L.; Rizzi, V.; Parrinello, M. Data-Driven Collective Variables for Enhanced Sampling. *J. Phys. Chem. Lett.* **2020**, *11* (8), 2998–3004. https://doi.org/10.1021/acs.jpclett.0c00535.

(42) Tribello, G. A.; Bonomi, M.; Branduardi, D.; Camilloni, C.; Bussi, G. PLUMED 2: New Feathers for an Old Bird. *Comput. Phys. Commun.* **2014**, *185* (2), 604–613. https://doi.org/10.1016/j.cpc.2013.09.018.